A rapid and controllable acoustothermal microheater using thin film surface acoustic waves

Yong Wang[a,b,c,d], Qian Zhang[a], Ran Tao[d,e], Dongyang Chen[a], Jin Xie[a,*], Hamdi Torun[d], Linzi E. Dodd[d], Jingting Luo[e], Chen Fu[e], Jethro Vernon[d], Pep Canyelles-Pericas[f], Richard Binns[d], and Yongqing Fu[d,a,*]

[a] The State Key Laboratory of Fluid Power and Mechatronic Systems, Zhejiang University, Hangzhou 310027, China

[b] Key Laboratory of 3D Micro/Nano Fabrication and Characterization of Zhejiang Province, School of Engineering, Westlake University, Hangzhou 310024, China

[c] Institute of Advanced Technology, Westlake Institute for Advanced Study, Hangzhou 310024, China

[d] Faculty of Engineering and Environment, University of Northumbria, Newcastle upon Tyne NE1 8ST, UK

[e] Shenzhen Key Laboratory of Advanced Thin Films and Applications, College of Physics and Optoelectronic Engineering, Shenzhen University 518060, China

[f] Department of Integrated Devices and Systems, MESA+ Institute, University of Twente, Enschede 7522NH, The Netherlands

* Corresponding authors: xiejin@zju.edu.cn; richard.fu@northumbria.ac.uk

ABSTRACT

Temperature control within a microreactor is critical for biochemical and biomedical applications. Recently acoustothermal heating using surface acoustic wave (SAW) devices made of bulk $LiNbO_3$ substrates have been demonstrated. However, these are generally fragile and difficult to be integrated into a single lab-on-a-chip. In this paper, we propose a rapid and controllable acoustothermal microheater using AlN/Si thin film SAWs. The device's acoustothermal heating characteristics have been investigated and are superior to other types of thin film SAW devices (e.g., ZnO/Al and ZnO/Si). The dynamic heating processes of AlN/Si SAW devices for both a sessile droplet and liquid within a polydimethylsiloxane (PDMS) microchamber were characterized. Results show that for the sessile droplet heating, the temperature at a high RF power is unstable due to significant droplet deformation and vibration, whereas for the liquid within the microchamber, the temperature can be precisely controlled by the input power with good stability and repeatability. In addition, an improved temperature uniformity using the standing SAW heating was demonstrated as compared to that of the travelling SAWs. Our work shows that the AlN/Si thin film SAWs have a great potential for applications in microfluidic heating such as accelerating biochemical reactions and DNA amplification.

Keywords: Acoustothermal heating, AlN thin film, Surface acoustic waves, PDMS chamber

1. Introduction

Lab-on-a-chip systems have attracted great attention for biochemical and biomedical applications due to their low reagent consumption, high efficiency and throughput, enhanced sensitivity and compact size [1, 2]. Recently, various biochemical and bioanalytical functions, including DNA sequencing [3], protein analysis [4], cell lysis [5] and drug screening [6] have been implemented into a lab-on-a-chip platform. A microreactor is one of the most important components in a lab-on-a-chip platform for biochemical analysis, where an elevated temperature is often required for the reactions leading to an increasing demand to integrate with a miniaturized heating system for heat generation and temperature control [7-9]. Various technologies have been developed for microfluidic heating such as Joule heating, microwave heating and infrared (IR) radiation heating [10-12]. Among them, Joule heaters integrated with microfluidic

chips are the most commonly used methods for microfluidic heating. However, their heating/cooling rates are limited by the thermal inertia of the heating block, and sometimes patterning of metallic heaters on the analytical areas of the chip increases the cost and complexity of the system [13, 14]. Compared to Joule heating, microwave heating has advantages of low thermal inertia and high energy density, making it suitable for rapid thermal cycling [15]. However, an appropriate impedance matching between the reaction solutions and microwave resonator is required. This method is also limited to a narrow range of volumes and microwave frequencies. IR radiation heating enables a rapid, non-invasive and selective heating of the liquid, but the heating is often localized at a certain small area, thereby generating a poor temperature uniformity [16]. Moreover, the IR heating usually requires a bulky and expensive source, making them impractical for disposable or portable uses.

Recently surface acoustic waves (SAWs) have also been explored for microfluidic heating due to their significantly acoustothermal heating effects [17-20]. In comparison with the above methods, SAW heating technologies have obvious advantages such as low cost, low power consumption, miniaturization and easy implementation [21, 22]. In addition, the interaction between the SAW and the liquid can induce the internal streaming within the liquid [23-25], thereby enhancing the heat transfer by forced convection and leading to a uniform temperature distribution [26]. At present, certain types of biochemical and biomedical applications including synthetic chemistry, blood coagulation monitoring and polymerase chain reactions (PCRs) have been implemented using SAW heating technologies [27-29]. Conventional acoustothermal heating devices are mostly made on bulk $LiNbO_3$ substrates due to their large piezoelectric constant and electromechanical coupling coefficients (5~11%) [16, 30-32]. However, these bulk piezoelectric substrates are fragile and easily broken under a large thermal/electric shock. They are also difficult to couple with other microfluidic substrates for integration with interface electronics for signal processing [33, 34]. In comparisons, thin film SAW technologies, such as those based on ZnO or AlN thin films, have significant advantages including suitability for flexible electrode designs, good tolerance to high voltage/power, good thermal stability (e.g., AlN films can maintain good piezoelectric properties in air up to 700℃) and easy integration with microelectronics [30, 35]. Another key advantage using piezoelectric thin films is that they can be easily deposited onto various substrates such as silicon, glass, metal and polymer to realize new functions [25]. When piezoelectric films are deposited onto silicon substrate, the fracture or cracking of the SAW devices has seldomly been observed even at a high RF power of 60~70 W for up to a few minutes, mainly due to the high thermal conductivity and good fracture strength of the polished Si substrate [34]. These properties are desirable for microfluidic heating applications. However, to date, the acoustothermal heating characteristics of thin film SAW devices have not been systematically investigated.

In this paper, we investigate acoustothermal heating characteristics of AlN and ZnO thin film-based SAW devices and compare their heating performances. We have proposed a PDMS based thin film SAW acoustothermal microheater and realized digital control of microfluidic heating temperature. The leaky SAWs absorbed by the PDMS are compressional bulk waves, and they can efficiently heat the chamber in a volumetric nature, making it simultaneously as a liquid reservoir and heater, thereby achieving a high heating temperature nearly 100℃ with good stability and repeatability.

2. Materials and methods

AlN films of ~4.7 μm thick were deposited onto 4-inch silicon (100) substrate and ZnO films of ~5 μm thick were deposited onto 4-inch silicon (100) substrate and polished Al plate substrate using a DC magnetron sputtering processes. The thickness of silicon substrate is 500 μm. The thickness of polished Al plate substrate is 1500 μm, with a root mean square (RMS) roughness of ~19 nm (see Fig. S1 in the supporting information). For AlN film deposition, a high-purity (99.999%) aluminum target (4 inches in diameter) was used, and it was kept with a 50 mm distance from the sample holder. Before the deposition, the silicon substrate was heated to 400℃ in the sputter chamber with a base pressure of 1 ×

10^{-8} Torr. Then the surface of substrate holder was plasma-cleaned by means of a short bombardment (60s) with Ar^+ ions from a bias RF glow discharge. After that, the AlN films were deposited onto silicon substrate with an Ar/N_2 gas flow rate of 4/6 sccm, a chmaber pressure of 1.9 mbar, a DC target power of 1200 W and a platen temperature of 400℃ [36]. During deposition, an RF bias power of 80 W was applied to the substrate in order to increase film adhesion to the substrate and reduce in-plane film stress. For ZnO film deposition, a zinc target with a purity of 99.999% was used. ZnO films were deposited onto substrates using an Ar/O_2 gas flow rate of 10/13 sccm, a DC target power of 400 W and a pressure level of 6.5 mbar without substrate heating [37]. The distance between the zinc target and the sample holder was 70 mm. Moreover, the sample holders were rotated during the deposition to obtain uniform AlN and ZnO thin films.

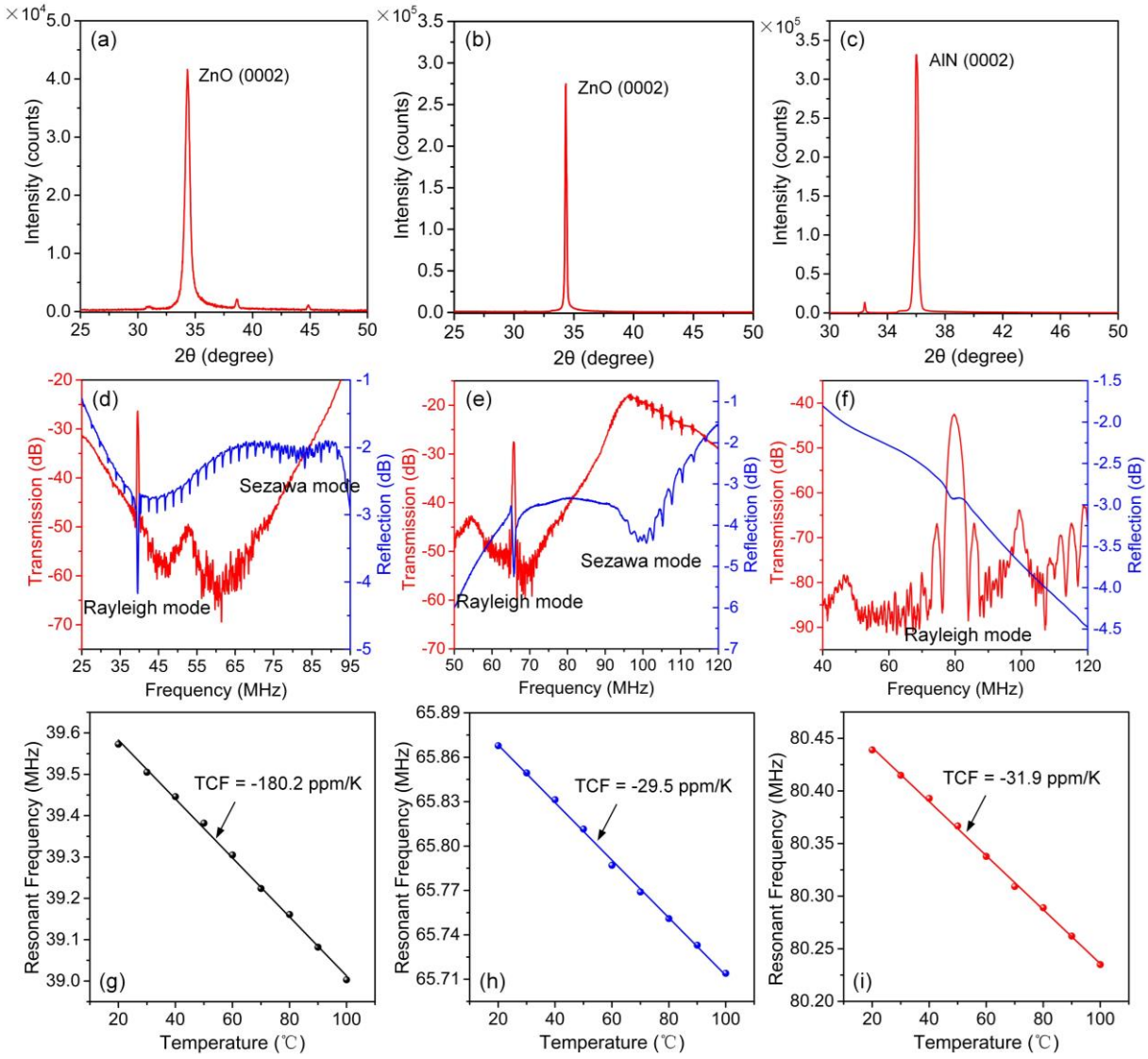

Fig. 1. XRD spectra of (a) ZnO films on Al plate substrate, (b) ZnO films on silicon substrate and (c) AlN films on silicon substrate. Signal transmission and reflection spectra of the SAW devices for (d) ZnO/Al, (e) ZnO/Si and (f) AlN/Si. Resonant frequency changes as a function of temperature for (g) ZnO/Al SAW device, (h) ZnO/Si SAW device and (i) AlN/Si SAW device.

X-ray diffraction analysis shows that all the deposited ZnO and AlN films have good c-axis (0002) crystal orientations, as shown in Figs. 1(a-c). SAW delay lines with interdigital transducers (IDTs) were fabricated on the prepared substrates of AlN/Si, ZnO/Si and ZnO/Al using the conventional photolithography and lift-off processes. The thicknesses of the electron beam evaporated Cr/Au electrodes were 20/100 nm. Each IDT of the SAW devices was composed of 40 pairs of fingers, with a spatial periodicity of 64 μm and an acoustic aperture of 4.9 mm. The resonant

characteristics of the fabricated SAW devices were characterized using a network analyzer (Agilent E5061B), with reflection and transmission spectra shown in Figs. 1(d-e). As the device wavelength (λ = 64 μm) is smaller than the substrate thickness, all the SAW devices have generated the Rayleigh wave mode, which was used for acoustothermal heating. For investigating the effect of frequency shift caused by acoustothermal heating, the temperature coefficient of frequency (TCF) of the SAW device was measured. The measured TCF values for AlN/Si, ZnO/Si and ZnO/Al SAW devices are -31.9 ppm/K, -29.6 ppm/K and -180.2 ppm/K, respectively, as shown in Figs. 1(g-i). The electromechanical coupling coefficients of the SAW devices were calculated based on the Smith Charts at the central resonant frequencies [38]. The calculated electromechanical coupling coefficients for AlN/Si, ZnO/Si and ZnO/Al SAW devices are about 0.24%, 1.08% and 1.56%, respectively. The PDMS microchamber was fabricated using a standard soft photolithography process [13, 39]. The microchamber defines a liquid reservoir that is 2000 μm in length, 4000 μm in width, and 1200 μm in height, resulting in a total volume of 9.6 μL. The enclosing PDMS chamber is about 400 μm in thickness.

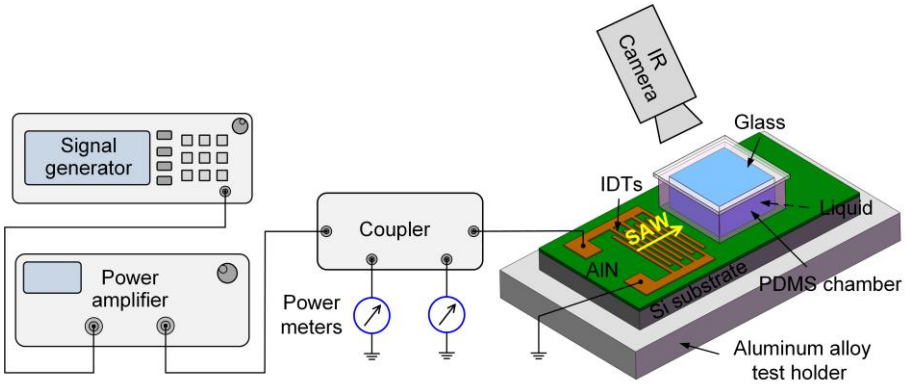

Fig. 2. Schematic of experimental setup for microfluidic heating within a PDMS microchamber.

Fig. 2 shows the schematic of the experimental setup for microfluidic heating. An RF signal was generated using a signal generator (Marconi 2024) and amplified using a power amplifier (Amplifier research, 75A250). The amplified signal was then fed into the input IDTs via a coupler. The incident power and reflected power of the SAW device were measured using two power meters connected to the coupler. The real input SAW power was determined by the power difference between two power meters. For microfluidic heating, the SAW devices were placed on an aluminum alloy test holder to increase the heat dissipation. To restrict the liquid movement, a PDMS chamber was bonded onto the device surface to hold the liquid. A glass cover with the thickness of ~50 μm was placed on the top of the chamber to reduce evaporation. The liquid temperature within the PDMS chamber after applying an RF power was measured in real time using an infrared video camera (ThermaCAM^{TM} SC640, with a spatial resolution of 200 μm). For each test, the IR camera was calibrated based on the emissivity of the object, and the results was also verified by using a thermocouple which was put inside the PDMS microchamber. The photograph of the experiment setup for microfluidic heating is shown in Fig. S2 in the supporting information.

3. Results and discussion

3.1. Acoustothermal heating

Figs. 3(a-c) compare acoustothermal heating characteristics of different thin film SAW devices (without any liquid) under different input SAW powers. When an RF signal is applied to the SAW device, the device temperature is rapidly increased. With the increase of duration of the applied power, the device temperature gradually reaches a nearly stable state due to the thermal equilibrium between the SAW device heating and heat dissipation from the aluminum alloy bulk holder and the surrounding air. There are still minor increases in the device temperature with the duration of the applied power, mainly due to the gradual heat accumulation within the cooling substrate. For all the thin film SAW devices, the

device temperature is increased with the increase of input power. At the same input power, the AlN/Si SAW device presents the highest heating temperature when compared to those of ZnO thin film-based SAW devices. This is probably due to its lower value of the electromechanical coupling coefficient (0.24%), which results in more applied power transformed into the heat. In addition, the ZnO/Al SAW device shows a lower heating temperature than that of ZnO/Si SAW device due to a higher thermal conductivity of Al plate.

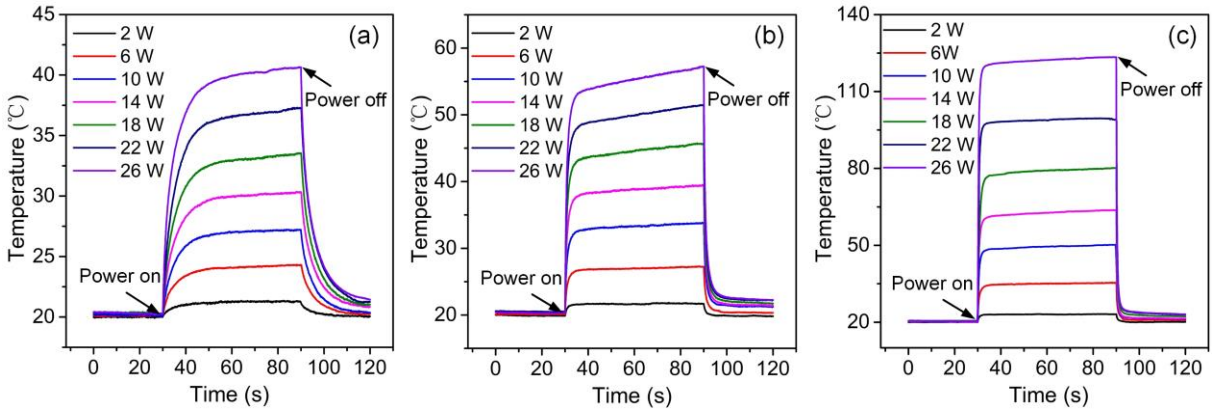

Fig. 3. Temperature evolution of the device at the same position (at the center of acoustic aperture and near the input IDT) as a function of duration for (a) ZnO/Al SAW device, (b) ZnO/Si SAW device and (c) AlN/Si SAW device under different input SAW powers.

Table 1. Comparisons of average heating/cooling rates for different SAW devices under different input powers.

Input power (W)	Average heating rate (℃/s)			Average cooling rate (℃/s)		
	AlN/Si	ZnO/Si	ZnO/Al	AlN/Si	ZnO/Si	ZnO/Al
2	1.64	0.76	0.12	1.76	0.56	0.11
6	4.74	1.63	0.26	5.49	1.47	0.32
10	8.41	2.82	0.42	9.15	2.33	0.54
14	10.46	3.54	0.53	13.12	3.09	0.67
18	14.15	4.15	0.66	17.71	4.03	0.82
22	21.93	4.79	0.87	21.52	4.48	0.98
26	28.07	5.75	1.11	27.36	5.32	1.25

The average values of heating/cooling rates for different thin film SAW devices under different input powers are summarized in Table 1. The average heating/cooling rate of the SAW device is defined as the temperature changes divided by the time from the start of heating or cooling to a relatively stable state of the temperature. Results show that the AlN/Si SAW device presents a much higher heating/cooling rate than those of ZnO thin film-based SAW devices. Therefore, in comparison with ZnO thin film SAW devices, AlN thin film SAW device has a better heating performance in terms of heating temperature, heating rate or temperature stability. In the next sections, we will focus on microfluidic heating characteristics using the AlN/Si SAW device.

3.2. Frequency effect on heating performance

The SAW devices are usually operated at their corresponding resonant frequencies for heating applications. However, the device's resonant frequency will be shifted due to temperature changes caused by the acoustothermal heating, and this will influences the heating performance of the device. For investigating the effect of frequency shift caused by acoustothermal heating on the device heating performance, the AlN/Si SAW device was excited at different frequencies near the nominal resonant value (80.44 MHz), and the obtained temperature results shown in Fig. 4. When the device was excited at 75 MHz and 85 MHz, a temperature deviation of about 0.7~1.3℃ was observed when

compared to that value of the nominal resonant frequency. In this study, the maximum heating temperature was below 150℃, the measured TCF for the AlN/Si SAW device is about -31.9 ppm/℃, corresponding to a frequency shift of smaller than 0.34 MHz during the heating process. As the device's frequency change caused by the acoustothermal heating is not significant, the effect of frequency shift during the heating process on device heating performance is negligible.

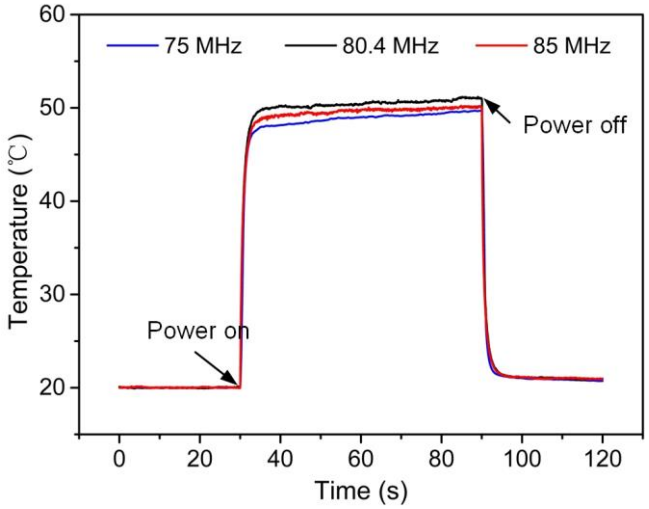

Fig. 4. Temperature evolution of the device substrate at the same position as a function of duration for AlN/Si SAW device (with a resonant frequency of 80.44 MHz) excited using different frequencies with an input power of 10 W.

3.3. Microfluidic heating

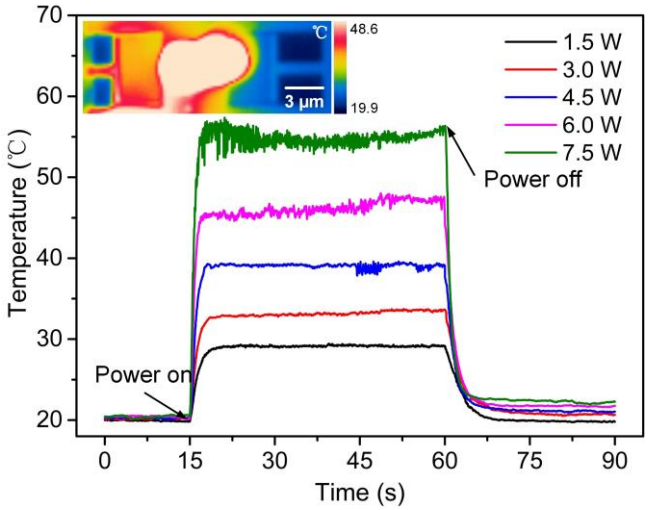

Fig. 5. Temperature evolution of the droplet (10 μL) as a function of duration under different input SAW powers, the insert shows the deformation and vibration of the droplet caused by SAW agitation effects.

The heating characteristics of the microfluidics were evaluated starting with the heating of the sessile water droplet using the AlN/Si SAW device. As shown in Fig. 5, when the SAWs propagate into the water droplet, the average temperature within the droplet is increased quickly. After a duration of ~4s, the droplet temperature reaches a steady state with a thermal equilibrium determined by the dynamics of the SAW heating and heating dissipation across the cooling substrate and the air. The temperature increases steadily with the input SAW power until the droplet becomes deformed and unstable due to significant acoustic agitation effects, then the measured temperature starts fluctuation. The observed

significant vibration and deformation of the droplet are shown in the insert of Fig. 5. In addition, the significant heating of the droplet causes the evaporation [40, 41], thereby leading to a reduction in liquid volume. Therefore, for the sessile droplet heating without taking into account of the surface treatment, droplet anchoring and droplet coating strategies, it is difficult to gain a stable condition of high temperature at the high power.

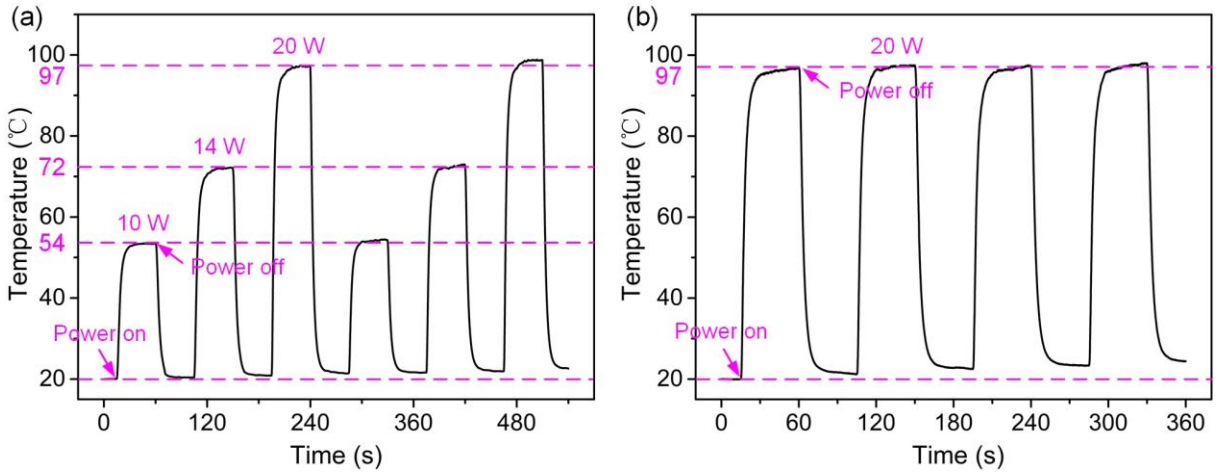

Fig. 6. (a) Temperature evolution of the liquid within the PMDS microchamber under different power cycles using the AlN/Si SAW device and (b) the stability and repeatability of the heating temperature using the AlN/Si SAW device under the same power cycles.

For realizing stable and repeatable control of liquid heating temperature using the SAW device, a PDMS chamber was adopted to store the liquid, as illustrated in Fig. 2. As the leaky SAWs absorbed by the PDMS chamber are compressional bulk waves, the liquid within the PDMS chamber can be efficiently heated in a volumetric nature [13]. Fig. 6(a) shows the heating temperatures for liquid within the PDMS microchamber under different power cycles. The liquid heating temperature can be controlled by the input SAW power, and periodic thermal cycles for potential PCR applications have been demonstrated using the AlN/Si thin film SAW based acoustothermal microheater. Moreover, as shown in Fig. 6(b), the heating temperature for liquid within the PDMS microchamber has also shown a good stability and repeatability. The maximum heating temperature for the microfluidics demonstrated here reaches ~100℃, meeting the heating requirement for most biochemical reaction applications.

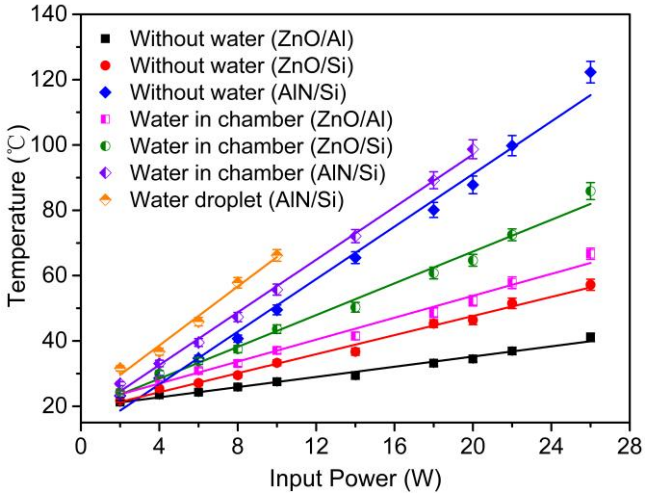

Fig. 7. Heating temperature comparisons for different thin film SAW devices using different heating forms under different input SAW powers. The temperatures were measured after the RF power was applied with a duration of 1 min.

Fig. 7 summarizes the average values of the heating temperatures for thin film SAW devices using different heating conditions. The temperatures of acoustothermal heating for both the device and microfluidics are linearly increased with

the increase of input SAW power. Since the applied power is proportional to the square of the applied voltage, the heating temperature is proportional to the square of the applied voltage, which is in a good agreement with the results reported in previous studies [17]. In addition, the liquid temperatures induced by the SAW device heating are larger than the temperature of acoustothermal heating of the device (without any liquid) under the same power. This is because the radiation of longitudinal waves into the liquid produces a significant acoustic wave heating effect besides the thermal transfer from the device substrate and the PDMS chamber to heat the liquid [13, 42]. Moreover, the temperature of SAW heating for liquid within the PDMS chamber is slightly lower than that of the sessile droplet at the same power, mainly due to the partial loss of acoustic energy into the walls of PDMS chamber [43].

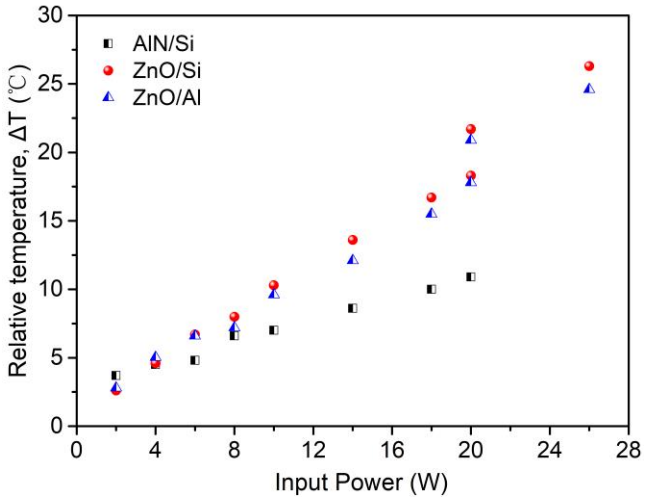

Fig. 8. Relative temperature of the liquid to device substrate for thin film SAW devices under different input SAW powers.

Fig. 8 shows relative temperatures of the liquid to device substrate for thin film SAW devices under different input SAW powers. The relative temperature of the liquid to device substrate is defined as the difference between the temperature of the liquid within the PDMS chamber induced by the SAW device heating and the temperature after the acoustothermal heating of the device. At the same power, the relative temperature of the liquid to device substrate for AlN/Si SAW device is smaller than those of ZnO/Al and ZnO/Si SAW devices due to its lower electromechanical coupling coefficients and thus a weaker acoustic wave heating effect. As previously explained, the electromechanical coupling coefficients for AlN/Si, ZnO/Si and ZnO/Al SAW devices are approximately 0.24%, 1.08% and 1.56%, respectively. A lower electromechanical coupling coefficient results in more applied power transformed into the heat, thereby achieving a higher heating temperature for the substrate. However, it will also lead to less acoustic wave generation, thereby weakening the heating effect by the acoustic waves. This is also the reason that a higher threshold microfluidic actuation power is needed for AlN thin film SAWs when compared to those of ZnO thin film SAWs [25]. Therefore, for microfluidic heating by the AlN/Si SAW device, the temperature rise within the liquid is mainly attributed to the thermal transfer from the acoustothermal heating of the device. However, for microfluidic heating by the ZnO thin film SAW devices, both the acoustic wave heating from radiation of longitudinal waves into the liquid and thermal transfer from acoustothermal heating of the device play important roles.

3.4. Temperature distribution and uniformity

For evaluating the temperature uniformity of the SAW based microfluidic heating, we further investigated the temperature distribution on the device surface (without any liquid). Fig. 9(a) shows the temperature distribution on the device surface in the SAW propagation direction, which was heated using the travelling wave of the AlN/Si SAW device. The substrate temperature was measured after the RF power was applied for 1 min. With the increased distance from the input IDTs, the temperature of the device substrate is linearly decreased. This is probably due to the propagation loss of

the travelling waves and increased thermal dissipation in the SAW propagation direction. The temperature distribution on the device surface along the direction of acoustic aperture was also obtained, and the results are shown in Fig. 9(b). The substrate temperature was measured after an RF power of 8 W was applied with a duration of 1 min. Results show that the SAW heating is significant in the center of acoustic aperture, which is the same with the results reported in a previous study based on $LiNbO_3$ SAW devices [44]. Therefore, there is a temperature gradient on the device surface using the travelling SAW induced heating.

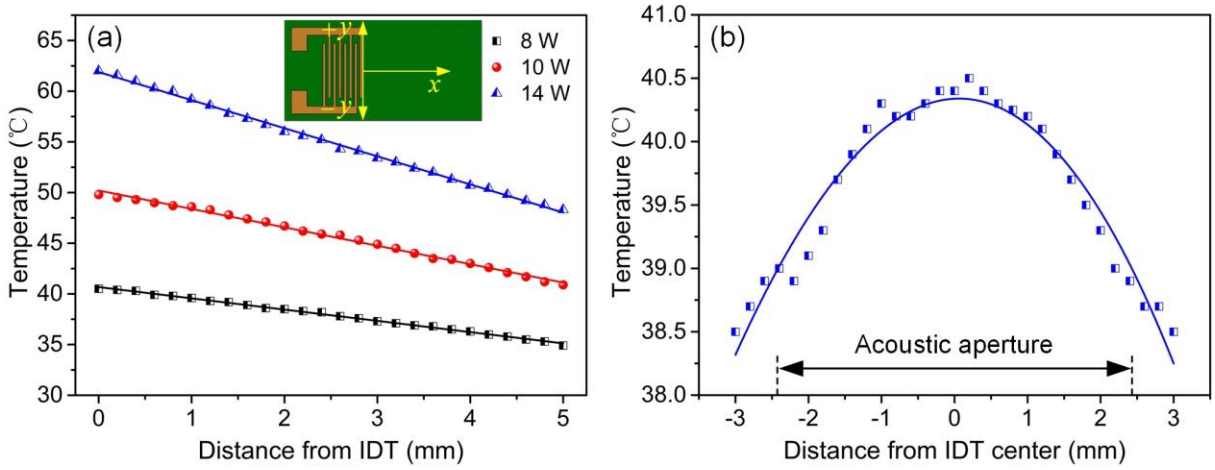

Fig. 9. (a) Device substrate temperature changes as a function of distance from the input IDTs (in the SAW propagation direction) heated using the traveling wave of the AlN/Si SAW device and (b) device substrate temperature changes as a function of distance from the center of acoustic aperture (perpendicular to the SAW propagation direction) with an input power of 8 W.

To improve the temperature uniformity of the microfluidic heating, the standing SAW (SSAW) design was further applied. For generating the SSAW, a power splitter was connected to the coupler output to generate two same RF signals. Meanwhile, the temperature standard deviation is used to quantify the temperature uniformity of the SAW based microfluidic heating. The lower the value of the temperature standard deviation, the better the temperature uniformity.

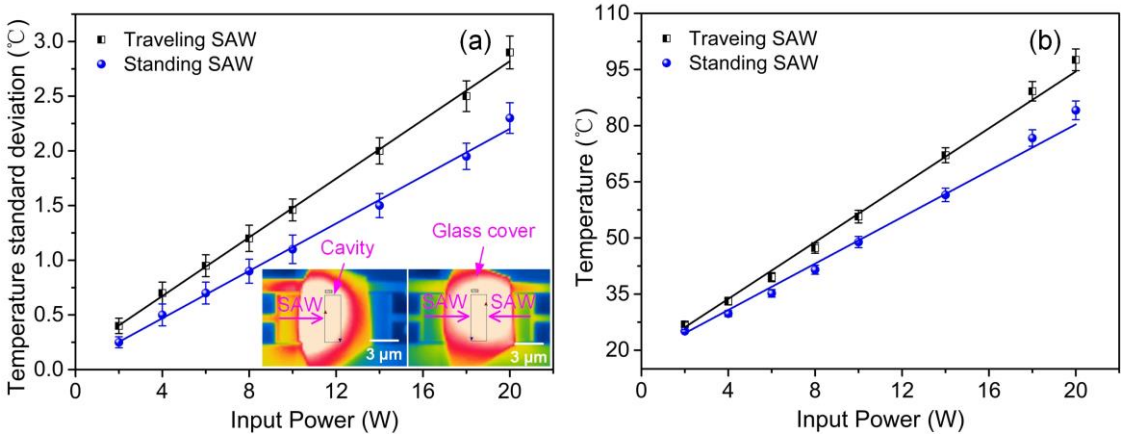

Fig. 10. (a) Temperature standard deviations of the liquid within the PDMS chamber for the travelling SAW heating and the SSAW heating under different input SAW powers and (b) liquid heating temperatures for the travelling SAW and the SSAW under different input SAW powers.

Fig. 10(a) compares temperature standard deviation of the liquid within the PDMS microchamber between the traveling SAW heating and the SSAW heating under different input SAW powers. The temperature standard deviation of the liquid increases with the increase of input SAW power. At the same power, the temperature standard deviation for the SSAW induced heating is lower than that of the traveling SAW heating due to its more concentrated acoustic field [19].

Therefore, the SSAW induced heating can generate a more uniform temperature within the liquid compared to that of the travelling SAW. The temperature uniformity of the microfluidics can be further improved by increasing pairs of IDTs, device wavelength or reducing the size of the PDMS chamber. An increased IDT wavelength can produce a longer SAW attenuation length in liquid [45, 46]. The SAW attenuation length reflects the interaction distance between the SAW and the liquid. A longer SAW attenuation length and a smaller size of PDMS chamber enhance the fluid streaming and mixing, thereby improving the temperature uniformity. However, it should be noted that the liquid heating temperature using the SSAW is slightly smaller than that of the travelling SAW at the same power, as shown in Fig. 10(b), probably due to the increased reflection of acoustic energy by the walls of the PDMS chamber.

4. Conclusions

In summary, we have proposed a thin film SAW based acoustothermal microheater and realized rapid and controllable microfluidic heating within a PDMS microchamber with good stability and repeatability. We investigated acoustothermal heating characteristics of different thin film (including ZnO/Al, ZnO/Si and AlN/Si) SAW devices and demonstrated better heating performance using the AlN/Si SAW device. Based on the AlN/Si SAW device, we further analyzed dynamic heating processes of the SAW device for the sessile droplet and liquid within the PDMS microchamber. Results show that for the heating of the sessile droplet without any droplet anchoring methods, it is difficult to reach a stable state of high temperature due to significant SAW agitation effects at a high RF power. However, for the liquid within the PDMS chamber, stable and repeated thermal cycles have been demonstrated and the heating temperature can be digitally controlled by the input SAW power with a maximum value approaching 100℃. Moreover, we have demonstrated an improved temperature uniformity using the SSAW induced heating effect.

Acknowledgements

This work was supported by the “Zhejiang Provincial Natural Science Foundation of China (LZ19E050002)” and the “National Natural Science Foundation of China (51875521, 51605485 and 51575487)”, Engineering Physics and Science Research Council of UK (EPSRC EP/P018998/1) and UK Fluidic Network (EP/N032861/1)- Special Interest Group of Acoustofluidics, and Newton Mobility Grant (IE161019) through Royal Society and NFSC.

References

[1] D. Mark, S. Haeberle, G. Roth, F. von Stetten, and R. Zengerle, “Microfluidic lab-on-a-chip platforms: requirements, characteristics and applications,” *Chem. Soc. Rev.*, vol. 39, no. 3, pp. 1153–1182, 2010.

[2] J. P. Lafleur, A. Jönsson, S. Senkbeil, and J. P. Kutter, “Recent advances in lab-on-a-chip for biosensing applications,” *Biosens. Bioelectron.*, vol. 76, pp. 213-233, 2016.

[3] C. Zhu, A. Hu, J. Cui, K. Yang, X. Zhu, Y. Liu, G. Deng, and L. Zhu, “A lab-on-a-chip device integrated DNA extraction and solid phase PCR array for the genotyping of high-risk HPV in clinical samples,” *Micromachines*, vol. 10, no. 8, pp. 537, 2019.

[4] K. L. Saar, Y. Zhang, T. Müller, C. P. Kumar, S. Devenish, A. Lynn, U. Łapińska, X. Yang, S. Linse, and T. P. Knowles, “On-chip label-free protein analysis with downstream electrodes for direct removal of electrolysis products,” *Lab Chip*, vol. 18, no. 1, pp. 162-170, 2018.

[5] S. H. Huang, L. Y. Hung, and G. B. Lee, “Continuous nucleus extraction by optically-induced cell lysis on a batch-type microfluidic platform,” *Lab Chip*, vol. 16, no. 8, pp. 1447-1456, 2016.

[6] D. T. Phan, X. Wang, B. M. Craver, A. Sobrino, D. Zhao, J. C. Chen, L.Y. Lee, S. C. George, A. P. Lee, and C. C. Hughes, “A vascularized and perfused organ-on-a-chip platform for large-scale drug screening applications,” *Lab Chip*, vol. 17, no. 3, pp. 511-520, 2017.

[7] A. Pandey, and A. Pandey, "Reverse micelles as suitable microreactor for increased biohydrogen production," *Int. J. Hydrog. Energy*, vol. 33, no. 1, pp. 273-278, 2008.

[8] M. Liu, C. Jia, Q. Jin, X. Lou, S. Yao, J. Xiang, and J. Zhao, "Novel colorimetric enzyme immunoassay for the detection of carcinoembryonic antigen," *Talanta*, vol. 81, no. 4, pp. 1625-1629, 2010.

[9] A. Sposito, V. Hoang, and D. L. DeVoe, "Rapid real-time PCR and high resolution melt analysis in a self-filling thermoplastic chip," *Lab Chip*, vol. 16, no. 18, pp. 3524-3531, 2016.

[10] K. R. Sreejith, C. H. Ooi, J. Jin, D. V. Dao, and N. T. Nguyen, "Digital polymerase chain reaction technology–recent advances and future perspectives," *Lab Chip*, vol. 18, no. 24, pp. 3717-3732, 2018.

[11] M. S. Boybay, A. Jiao, T. Glawdel, and C. L. Ren, "Microwave sensing and heating of individual droplets in microfluidic devices," *Lab Chip*, vol. 13, no. 19, pp. 3840-3846, 2013.

[12] J. H. Son, B. Cho, S. Hong, S. H. Lee, O. Hoxha, A. J. Haack, and L. P. Lee, "Ultrafast photonic PCR," *Light: Sci. Appl.*, vol. 4, no. 7, pp. e280, 2015.

[13] B. H. Ha, K. S. Lee, G. Destgeer, J. Park, J. S. Choung, J. H. Jung, J. H. Shin, and H. J. Sung, "Acoustothermal heating of polydimethylsiloxane microfluidic system," *Sci. Rep.*, vol. 5, pp. 11851, 2015.

[14] Y. Wang, Q. Zhang, D. Chen, R. Tao, Y. Guan, Z. Xu, Y. Fu, J. Xie, "Rapid and Controllable Digital Microfluidic Heating Using AlN/Si Rayleigh Surface Acoustic Waves," In *Pro. 33rd IEEE Int. Conf. Micro Electro Mech. Syst.*, Vancouver, Canada, Jan. 17-22, 2020, pp. 1098-1101.

[15] D. J. Marchiarullo, A. H. Sklavounos, K. Oh, B. L. Poe, N. S. Barker, and J. P. Landers, "Low-power microwave-mediated heating for microchip-based PCR," *Lab Chip*, vol. 13, no. 17, pp. 3417-3425, 2013.

[16] T. Roux-Marchand, D. Beyssen, F. Sarry, and O. Elmazria, "Rayleigh surface acoustic wave as an efficient heating system for biological reactions: investigation of microdroplet temperature uniformity," *IEEE Trans. Ultrason. Ferroelectr. Freq. Control*, vol. 62, no. 4, pp. 729-735, 2015.

[17] J. Kondoh, N. Shimizu, Y. Matsui, M. Sugimoto, and S. Shiokawa, "Development of temperature-control system for liquid droplet using surface acoustic wave devices," *Sens. Actuators A: Phys.*, vol. 149, no. 2, pp. 292-297, 2009.

[18] J. Qian, H. Begum, Y. Song, and J. E. Y. Lee, "Plug-and-play acoustic tweezer enables droplet centrifugation on silicon superstrate with surface multi-layered microstructures," *Sens. Actuators A: Phys.*, pp. 112432, 2020.

[19] Q. Y. Huang, Q. Sun, H. Hu, J. L. Han, and Y. L. Lei, "Thermal effect in the process of surface acoustic wave atomization," *Exp. Therm. Fluid Sci.*, vol. 120, pp. 110257, 2020.

[20] P. K. Das, A. D. Snider, and V. R. Bhethanabotla, "Acoustothermal heating in surface acoustic wave driven microchannel flow," *Phys. Fluids*, vol. 31, no. 10, pp. 106106, 2019.

[21] Y. Wang, Y. Wang, W. Liu, D. Chen, C. Wu, and J. Xie, "An aerosol sensor for PM1 concentration detection based on 3D printed virtual impactor and SAW sensor," *Sens. Actuators A: Phys.*, vol. 288, pp. 67-74, 2019.

[22] P. Delsing, A. N. Cleland, M. J. Schuetz, J. Knörzer, G. Giedke, J. I. Cirac, et al., "The 2019 surface acoustic waves roadmap," *J. Phys. D: Appl. Phys.*, vol. 52, no. 35, pp. 353001, 2019.

[23] J. Li, S. H. Biroun, R. Tao, Y. Wang, H. Torun, N. Xu, M. Rahmati, Y. Li, D. Gibson, C. Fu, J. Luo, L. Dong, J. Xie, and Y. Fu, "Wide range of droplet jetting angles by thin-film based surface acoustic waves," *J. Phys. D: Appl. Phys.*, vol. 53, no. 35, pp. 355402, 2020.

[24] S. Zahertar, Y. Wang, R. Tao, J. Xie, Y. Q. Fu, and H. Torun, "A fully integrated biosensing platform combining acoustofluidics and electromagnetic metamaterials," *J. Phys. D: Appl. Phys.*, vol. 52, no. 48, pp. 485004, 2019.

[25] Y. Wang, X. Tao, R. Tao, J. Zhou, Q. Zhang, D. Chen, H. Jin, S. Dong, J. Xie, and Y. Q. Fu, "Acoustofluidics along inclined surfaces based on AlN/Si Rayleigh surface acoustic waves," *Sens. Actuators A: Phys.*, vol. 306, pp. 111967, 2020.

[26] D. Beyssen, F. Sarry, and T. Roux-Marchand, "Correlation of heat transfers mechanism (s) and time constant equilibrium on digital Rayleigh-SAW microfluidic system," *Procedia Eng.*, vol. 120, pp. 1067-1070, 2015.

[27] K. Kulkarni, J. Friend, L. Yeo, and P. Perlmutter, “Surface acoustic waves as an energy source for drop scale synthetic chemistry,” *Lab Chip*, vol. 9, no. 6, pp. 754-755, 2009.

[28] N. Ohashin, and J. Kondoh, “Temperature control of a droplet on disposable type microfluidic system based on a surface acoustic wave device for blood coagulation monitoring,” *In Proc. IEEE Ultrasonics Symp*. pp. 1-4, 2015.

[29] J. Reboud, Y. Bourquin, R. Wilson, G. S. Pall, M. Jiwaji, A. R. Pitt, A. Graham, A. P. Waters, and J. M. Cooper, “Shaping acoustic fields as a toolset for microfluidic manipulations in diagnostic technologies,” *Proc. Natl. Acad. Sci.*, vol. 109, no. 38, pp. 15162-15167, 2012.

[30] Y. Q. Fu, J. K. Luo, N. T. Nguyen, A. J. Walton, A. J. Flewitt, X. T. Zu, Y. Li, G. McHale, A. Matthews, E. Iborra, H. Du, and W. I. Milne, “Advances in piezoelectric thin films for acoustic biosensors, acoustofluidics and lab-on-chip applications,” *Prog. Mater. Sci.*, vol. 89, pp. 31-91, 2017.

[31] R. J. Shilton, V. Mattoli, M. Travagliati, M. Agostini, A. Desii, F. Beltram, and M. Cecchini, “Rapid and controllable digital microfluidic heating by surface acoustic waves,” *Adv. Funct. Mater.*, vol. 25, no. 37, pp. 5895-5901, 2015.

[32] J. Park, B. H. Ha, G. Destgeer, J. H. Jung, and H. J. Sung, “Spatiotemporally controllable acoustothermal heating and its application to disposable thermochromic displays,” *RSC Adv.*, vol. 6, no. 40, pp. 33937-33944, 2016.

[33] J. Zhou, X. Tao, J. Luo, Y. Li, H. Jin, S. Dong, J. Luo, H. Duan, and Y. Fu, “Nebulization using ZnO/Si surface acoustic wave devices with focused interdigitated transducers,” *Surf. Coat. Technol.*, vol. 367, no. 15, pp. 127-134, 2019.

[34] Y. J. Guo, A. P. Dennison, Y. Li, J. Luo, X. T. Zu, C. L. Mackay, P. Langridge-Smith, A. J. Walton, and Y. Q. Fu, “Nebulization of water/glycerol droplets generated by ZnO/Si surface acoustic wave devices,” *Microfluid. Nanofluid.*, vol. 19, no. 2, pp.273-282, 2015.

[35] Y. Q. Fu, J. K. Luo, X. Y. Du, A. J. Flewitt, Y. Li, G. H. Markx, A. J. Walton, and W. I. Milne, “Recent developments on ZnO films for acoustic wave based bio-sensing and microfluidic applications: a review,” *Sens. Actuators B: Chem.*, vol. 143, no. 2, pp. 606-619, 2010.

[36] J. Zhou, M. DeMiguel-Ramos, L. Garcia-Gancedo, E. Iborra, J. Olivares, H. Jin, J. K. Luo, A. S. Elhady, S. R. Dong, D. M. Wang, and Y. Q. Fu, “Characterisation of aluminium nitride films and surface acoustic wave devices for microfluidic applications,” *Sens. Actuators B: Chem.*, vol. 202, pp. 984-992, 2014.

[37] R. Tao, G. McHale, J. Reboud, J. M. Cooper, H. Torun, J. T. Luo, J. Luo, X. Yang, J. Zhou, P. Canyelles-Pericas, Q. Wu, and Y. Q. Fu, “Hierarchical nanotexturing enables acoustofluidics on slippery yet sticky, flexible surfaces,” *Nano lett.*, vol. 20, no. 5, pp. 3263-3270, 2020.

[38] W. R. Smith, H. M. Gerard, J. H. Collins, T. M. Reeder, and H. J. Shaw, “Analysis of interdigital surface wave transducers by use of an equivalent circuit model,” *IEEE Trans. Microwave Theory Tech.*, vol. 17, no. 11, pp. 856-864, 1969.

[39] Z. Cai, W. Qiu, G. Shao, and W. Wang, “A new fabrication method for all-PDMS waveguides,” *Sens. Actuators A: Phys.*, vol. 204, pp. 44-47, 2013.

[40] Y. Wang, Z. Xu, Y. Wang, and J. Xie, “A study on AIN film-based SAW attenuation in liquids and their potential as liquid ethanol sensors,” *Sensors*, vol. 17, no. 8, pp. 1813, 2017.

[41] J. M. Stauber, S. K. Wilson, B. R. Duffy, and K. Sefiane, “On the lifetimes of evaporating droplets with related initial and receding contact angles,” *Phys. Fluids*, vol. 27, no. 12, pp. 122101, 2015.

[42] T. Zheng, C. Wang, Q. Hu, and S. Wei, “The role of electric field in microfluidic heating induced by standing surface acoustic waves,” *Appl. Phys. Lett.*, vol. 112, no. 23, pp. 233702, 2018.

[43] L. Schmid, A. Wixforth, D. A. Weitz, and T. Franke, “Novel surface acoustic wave (SAW)-driven closed PDMS flow chamber,” *Microfluid. Nanofluid.*, vol. 12, no. 1, pp. 229-235, 2012.

[44] J. Kondoh, N. Shimizu, Y. Matsui, and S. Shiokawa, “Liquid heating effects by SAW streaming on the piezoelectric substrate,” *IEEE Trans. Ultrason. Ferroelectr. Freq. Control*, vol. 52, no. 10, pp. 1881-1883, 2005.

[45] Y. Wang, D. Chen, C. Wu, and J. Xie, “Effect of droplet boundary behaviors on SAW attenuation for potential microfluidic applications. *Jpn. J. Appl. Phys.*, vol. 58, no. 3, pp. 037001, 2019.

[46] M. Alghane, Y. Q. Fu, B. X. Chen, Y. Li, M. P. Y. Desmulliez, and A. J. Walton, “Frequency effect on streaming phenomenon induced by Rayleigh surface acoustic wave in microdroplets,” *J. Appl. Phys.*, vol. 112, no. 8, pp. 084902, 2012.